Composites: Part A 173 (2023) 107706

Contents lists available at ScienceDirect

Composites Part A

journal homepage: www.elsevier.com/locate/compositesa

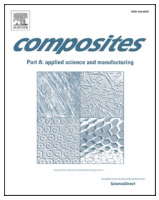

Effect of moisture absorption on curing of wind blades during repair

Sagar P. Shah, Michael N. Olaya, Evgenia Plaka, Joseph McDonald, Christopher J. Hansen, Marianna Maiarù *

University of Massachusetts Lowell, 1 University Ave, Lowell, MA 01854, USA

ARTICLE INFO

Keywords:
Wind energy
Structural repair
Environmental moisture
Process modeling
Heat transfer
Cure kinetics

ABSTRACT

Efficient structural repair of wind turbine blades is essential to reducing the Levelized Cost of Energy (LCOE) for wind energy. Repairs carried out up-tower are sensitive to environmental conditions whose effects on the material properties during processing need to be accounted for to accurately predict the repair outcome. This study investigates the effect of moisture content from environmental exposure on the cure kinetics of an infusion epoxy-amine resin system used in wind turbine blade manufacturing and repair and provides an experimentally validated finite element tool for the analysis of cure cycle repairs as a function of repair geometry and moisture content. Moisture absorption tests on the two-part infusion system reported up to 12% moisture uptake by the curing agent under high temperature and relative humidity conditions. Differential scanning calorimetric measurements of resin in the presence of moisture revealed an accelerated cure behavior. Numerical predictions of a repair model agreed well with the corresponding lab-scale repair and revealed a substantial temperature lag within the repair patch that resulted in thermal gradients and spatial distribution of the degree of cure. The repair geometry and the accelerated-cure kinetics greatly influenced the temperature and cure distribution within the repair. The proposed approach can be used to reduce turbine downtime by minimizing the curing time.

1. Introduction

State-of-the-art wind turbine blades are composed of thermoset fiber-reinforced polymer composites (FRPC) that provide high mechanical performance and are lightweight due to their excellent specific mechanical properties [1,2]. Over the last two decades, wind turbine size has progressively increased to harness wind energy in greater capacities and meet the global demand for increased production of sustainable energy [1,3]. During their operational life of about 20–25 years, wind turbine blades are exposed to a variety of adverse environmental conditions, including lighting strikes, extreme winds, rains, thermal cycles, and foreign object impacts, all of which result in material degradation and structural damage [2–5]. Repairs are fundamental to restoring structural integrity and aerodynamic efficiency of the blades to ensure reliable wind turbine operations after the damage has occurred [6]. The operation and maintenance (O&M) cost accounts for a staggering 25% of the total levelized cost per kWh produced over the lifetime of a turbine [7,8]. Repair procedures are highly dependent on the damaged area; when the repair size is manageable, the repair is performed up-tower in variable ambient conditions depending on the location, day, and time of the maintenance. Efficient and accurate computation techniques, able to predict the outcome of the repair and establish an optimized cure cycle that can ensure complete resin cure in minimum time, are needed to reduce the turbine downtime and increase the levelized cost of electricity (LCOE) for wind energy production.

After damage assessment and removal of the damaged substrate [1,3,6–8] the structural repair is performed by applying a scarf patch. The patch is made of a fiber-impregnated, viscous epoxy resin that needs to be cured within the parent laminate by applying temperature and pressure to restore the load-bearing capability of the material. Uniformity in the spatial distribution of the cure and temperature within the repair zone is critical to achieving high-quality repair. Aggressive cure cycles may lead to thermal gradients throughout the repair resulting in non-uniform curing of the constituent materials and overheating of the parent component, which may further introduce process-induced deformation, residual stress generation, and microcracking in the repair patch [1]. An in-depth understanding of the effect of processing parameters (including temperature ramp rates, hold temperature, and hold times) on the volumetric heat generation by the epoxy and distribution within the repair can avoid the aforementioned process-induced

* Corresponding author.
E-mail address: marianna_maiaru@uml.edu (M. Maiarù).

https://doi.org/10.1016/j.compositesa.2023.107706
Received 13 April 2023; Received in revised form 30 June 2023; Accepted 23 July 2023
Available online 24 July 2023

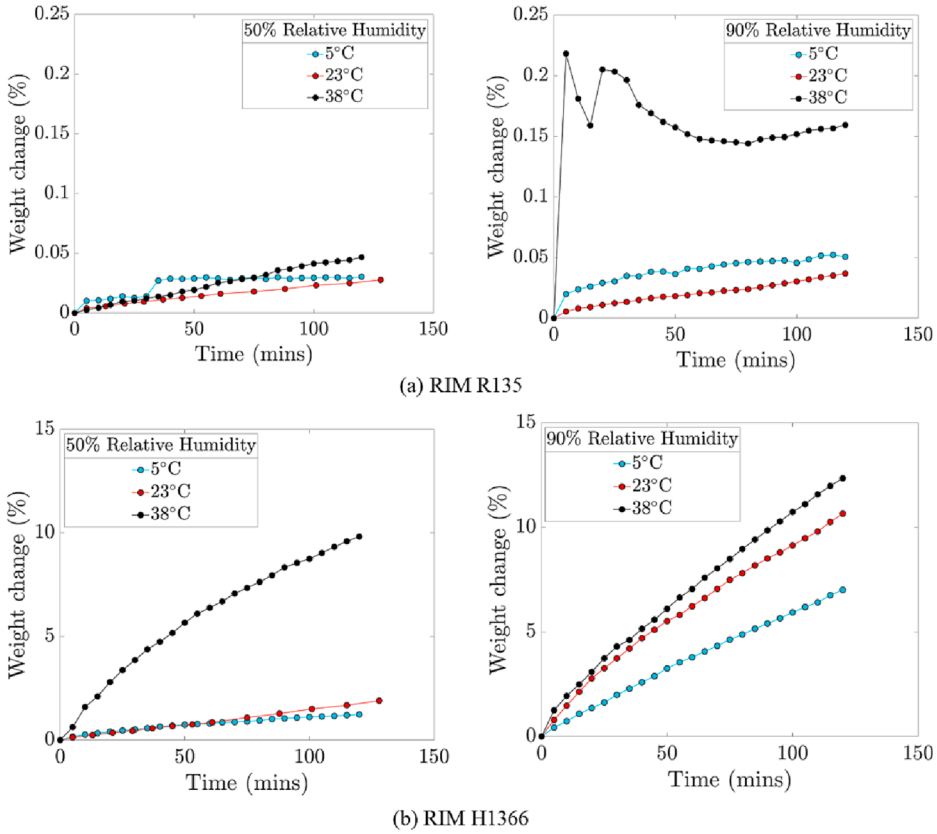

Fig. 1. Moisture absorption test results showing the percentage weight change in (a) base epoxy RIM R135 and (b) curing agent RIM H1366 when subjected to various temperature and relative humidity conditions. (For interpretation of the references to colour in this figure legend, the reader is referred to the web version of this article.)

Table 1
Percentage of moisture absorption by base epoxy RIM R135 and curing agent RIM H1366 when subjected to various environmental conditions.

Temperature (°C)	Relative humidity (%)	Moisture absorption (wt %)	
		RIM R135	RIM H1366
5	50	0.03	1.23
	90	0.05	7.01
23	50	0.04	3.07
	90	0.04	10.66
38	50	0.05	9.82
	90	0.22	12.35

defects in the repair patch and aid in achieving ultimate structural integrity of the blade in a time- and cost-effective manner [9].

Computational modeling of structural repair can facilitate the prediction and assessment of composite processing for any repair geometry under given environmental conditions and provide repair-specific optimized procedures to achieve the highest quality repair [7,8]. Various numerical approaches have reported the use of phenomenological kinetic models and three-dimensional heat transfer equations to predict cure evolution and temperature distribution during extensive blade repairs [6,10–16]. Several studies have also employed constitutive relations to predict residual stress generation and distribution, assess the effect of defects and repair imperfections on strength and the lifetime of repaired structures, and optimize repair patch and scarfed joint configurations [7,9,17–23]. While such studies provide valuable insight into blade repair procedures, an aspect often ignored is the environmental conditions under which the repair is performed and its influence on the epoxy resin reactivity and mechanical behavior. The altered chemistry of the epoxy resin due to environmental exposure – relative humidity and temperature, for instance – may warrant a completely different set of processing conditions (compared to the standard operating procedures) for an effective repair. Therefore, it is critical to evaluate the influence of environmental exposure on epoxy resin behavior before a repair is planned [1,24–27].

Several studies have reported the detrimental effect of moisture content on the polymeric resin's mechanical performance and reactivity [1,3,6,24–28]. Pre-cure moisture absorption in epoxy resins and adhesives is known to accelerate the autocatalytic curing reaction, which in turn affects the volumetric heat generation [6,25,26]. Moisture uptake by the epoxy resin is highly dependent on the environmental conditions during repair and the exposure time, which makes the determination of an optimized cure cycle for the repair extremely challenging. Furthermore, degradation of the resin strength and stiffness – due to phenomena such as reduction in the glass transition temperature, plasticization, and chemical swelling/degradation – resulting from moisture uptake is widely reported [1,24,26–28]. Finally, moisture absorption by the parent laminate and the repair patch can introduce voids during the repair's curing phase, which can lead to delamination, rendering the repair ineffective [3]. Therefore, the environmental and processing conditions and their influence on the structural integrity of the repair must be considered for a successful repair.

The objective of this study is to investigate the effect of moisture content from environmental exposure on the cure kinetics of an infusion resin system used in wind turbine blade manufacturing and repair and provide experimentally validated computational tools for the analysis of cure cycle repairs. First, the effect of moisture on epoxy resin cure kinetics is assessed by carrying out a series of moisture absorption tests where the two-part resin system is exposed to several environmental conditions. Subsequently, the resin cure kinetics is characterized for various moisture content cases. Informed by the acquired cure kinetic

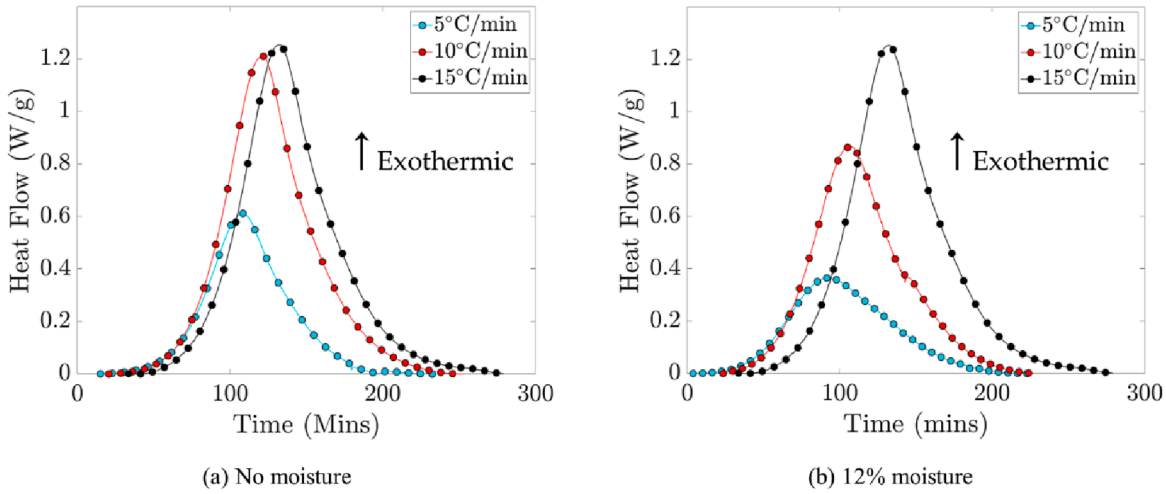

Fig. 2. Normalized heat flow versus time plots from dynamic DSC measurements taken at three different heating rates for (a) no moisture and (b) 12 wt% moisture content case. (For interpretation of the references to colour in this figure legend, the reader is referred to the web version of this article.)

Table 2
Cure kinetic modeling parameters for various moisture contents.

Moisture content (%)	Total heat of reaction H_T (J/g)	Kinetic constants			
		E_a (kJ/mol)	A (sec^{-1})	m (–)	n (–)
0	413.82	47	11,000	0.3	1.5
2	392.62	38	750	0.4	1.4
7	361.28	36	440	0.42	1.58
9	337.1	30	100	0.45	1.3
10	390.43	30	66	0.37	1.31
12	364.75	29	60	0.38	1.2

data, a 3D finite element (FE) curing model is implemented within the commercial software Abaqus using user-written subroutines to virtually cure a repair patch and predict the degree of cure and temperature evolutions during the procedure. Numerical results from the simulations are experimentally validated in terms of temperature distribution and degree of cure evolution. Lastly, the numerical model is used to understand the influence of repair geometry and environmental conditions on the spatial distribution of temperature and degree of cure within the repair.

This work is a milestone towards developing a computationally-based integrated computational materials engineering (ICME) framework for optimizing repair procedures that will improve the repair quality and ensure the repaired blade's long-term structural integrity. The focus of this manuscript is the prediction of the degree of cure and

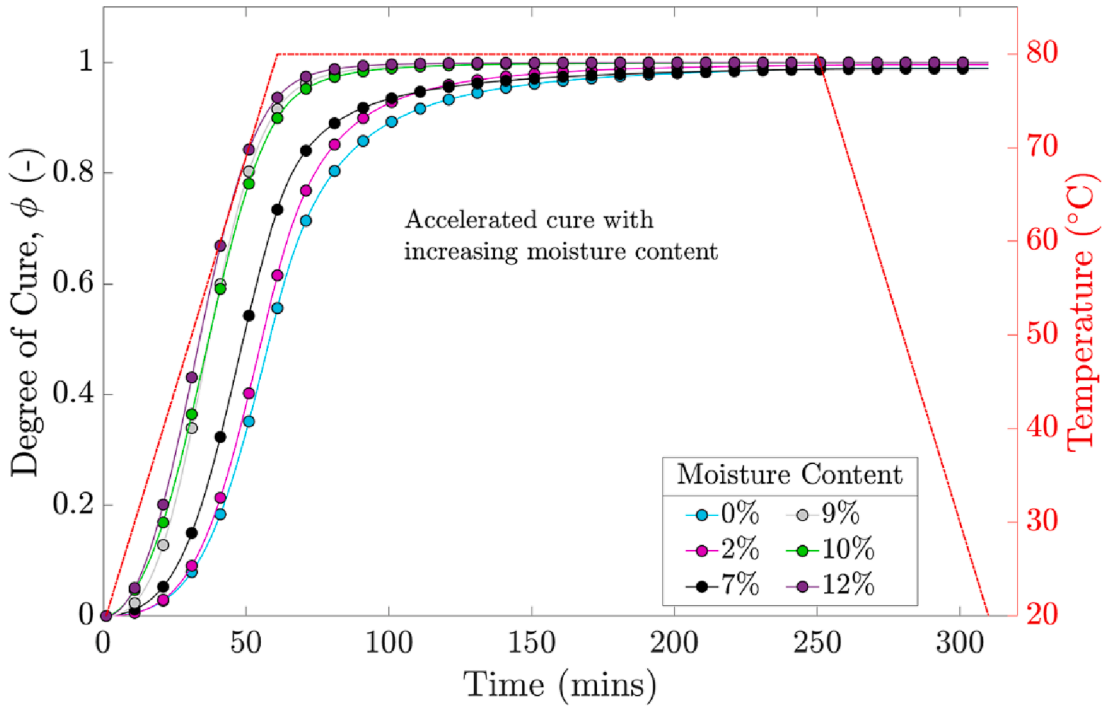

Fig. 3. Evolution of the degree of cure for the prescribed temperature profile as computed by the cure kinetic model for unconditioned (no moisture) and conditioned (various moisture content, 2%−12%) specimens. (For interpretation of the references to colour in this figure legend, the reader is referred to the web version of this article.)

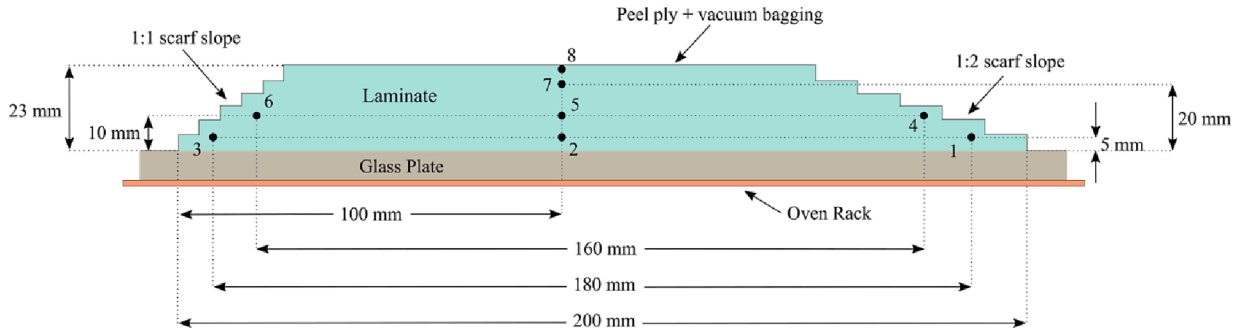

Fig. 4. Repair patch geometry for process modeling and lab-scale repair. (For interpretation of the references to colour in this figure legend, the reader is referred to the web version of this article.)

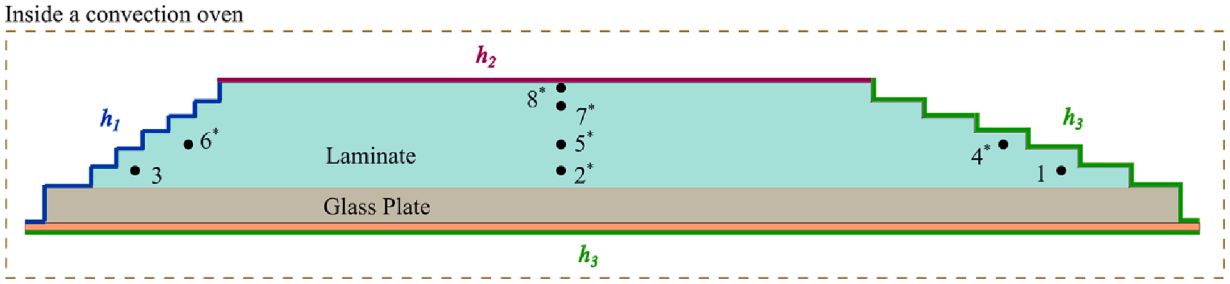

Fig. 5. Illustrations of the boundary conditions used for process modeling of the repair. Note that only thermocouples denoted with an asterisk (*) provided readable data. (For interpretation of the references to colour in this figure legend, the reader is referred to the web version of this article.)

Table 3
Constituent material properties used for the process modeling of the repair.

Material	Property		
	Density, ρ (g/cm^3)	Thermal conductivity k ($\times 10^{-4}$ W/mm-K)	Specific heat capacity c_p (J/g-K)
Borosilicate Glass Plate	2.23	12	1.5
Type 304 Stainless Steel	7.93	163	1.4
Patch Peel Ply Film	1.14	2.5	1.75
Vacuum Bag	1.14	2	1.3
RIM R135-H1366 (ϕ = 0)	1.20	1.59	1.35
RIM R135-H1366 (ϕ = 1)	1.20	2.45	1.62
E-glass Fiber	2.55	12	1.2

temperature evolutions during repair with the understanding that temperature and cure gradients affect the mechanical properties evolution of the epoxy resin and therefore residual stress generation [12]. The prediction of residual stress generation and mechanical performance after repair are not the subjects of this study. Future work will embed the curing models derived in this study within an ICME framework that links material models, structural models, and experiments at multiple length scales to obtain digital twins of the blade [9,21–23,29–37].

This manuscript is organized as follows: the methodology to study the influence of moisture on cure kinetics for resin infusion and their corresponding curing models are presented in Section 2. Modeling results and their validation for two different scarfing slopes and different moisture content are detailed in Section 3. The main conclusions are summarized in Section 4.

2. Methodology

During in-field repairs, the epoxy resin mixture may be exposed to environmental moisture for extended periods, which may be absorbed by the resin and alter the curing kinetics. First, the moisture absorption was quantified according to O&M instructions and in-field data. Then, the resin cure kinetics was characterized through Differential Scanning Calorimetry (DSC) for a widely used commercial epoxy system developed by Westlake Epoxy for wind energy applications: the infusion system EPIKOTE^{TM} Resin MGS RIMR 135 with EPIKURE^{TM} Curing Agent MGS RIMH 1366 (henceforth referred to as RIM R135-H1366). RIM R135-H1366 is a relatively low-viscosity system with an elevated curing temperature ideal for vacuum-assisted infusion processes. The system comprises bisphenol-A base epoxy resin with an amine-based curing agent. Unidirectional (UD) stitched E-glass fibers (areal weight of 955 g/m^2), manufactured by Saertex and distributed by Fibre Glast Developments Corp., were used as reinforcements. The moisture absorption tests are detailed in Section 2.1. Section 2.2 describes the cure kinetic characterization. The curing model implementation is discussed in Section 2.3.

2.1. Moisture absorption characterization

The moisture absorbed by the base epoxy and the curing agent during the repair was characterized by separately exposing the two constituents to environmental conditions encountered during in-field repairs. 60 g of RIM R135 epoxy samples and 20 g of RIM H1366 curing agent samples were placed inside the environmental chamber in separate cylindrical containers which were 2.5 in. in diameter and height. The chamber was set to several combinations of temperature (5 °C, 23 °C, and 38 °C) and relative humidity (RH of 50% and 90%). These conditions were based on the O&M instructions and in-field repair reports obtained from two in-field service repair companies. The initial specimen weight was recorded before the test, and subsequently, the specimens were weighed in five-minute intervals over a two-hour exposure period. This exposure window was also chosen based on the analysis of wind turbine repair reports. The relative percentage weight gain calculated for each data point in the sample reflected the moisture absorbed over the exposure period. These tests were conducted for one

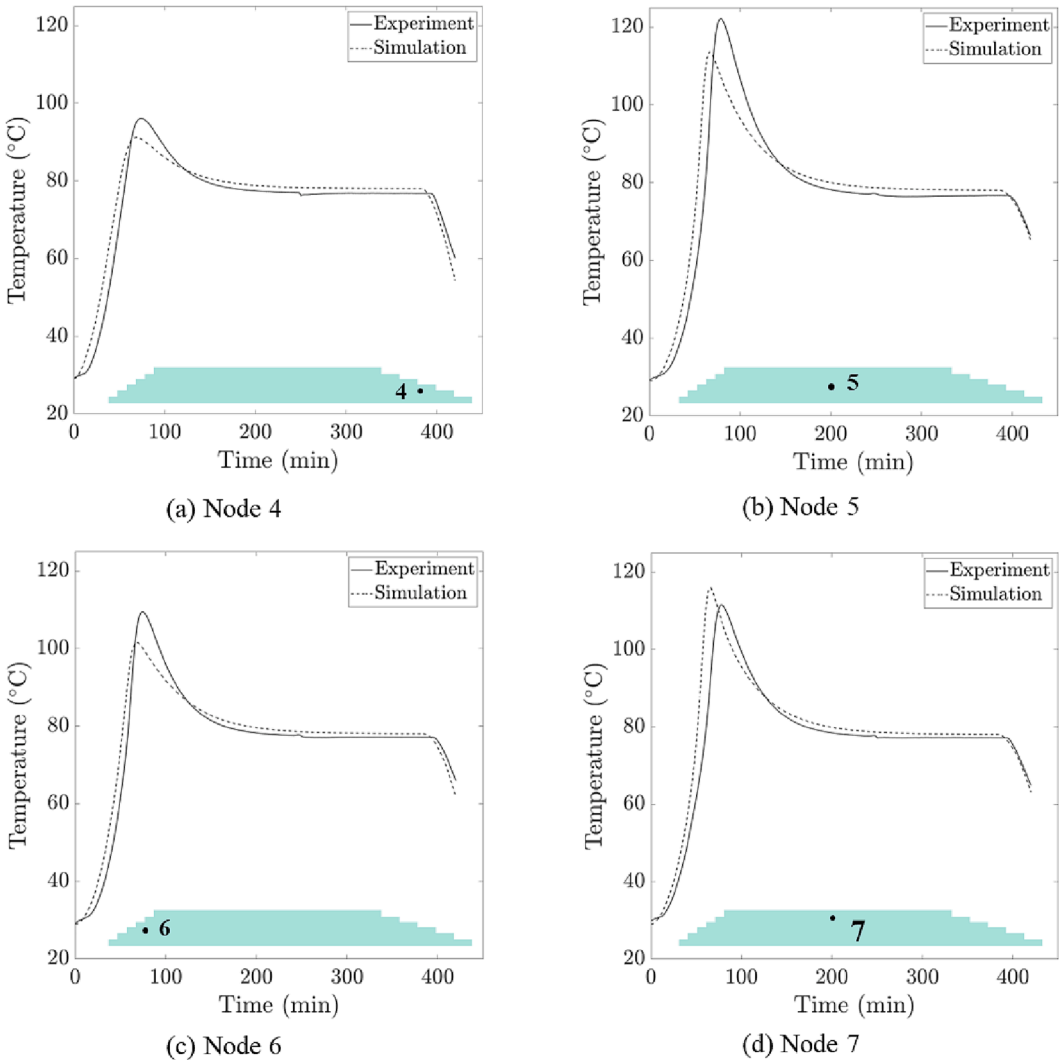

Fig. 6. Plots of temperature evolution in the repair patch as a function of the time for (a) node 4, (b) node 5, (c) node 6, and (d) node 7 from experiments and numerical model. (For interpretation of the references to colour in this figure legend, the reader is referred to the web version of this article.)

set of specimens per environmental condition.

Fig. 1 shows the moisture absorption test results for all six test conditions for both resin and curing agent. For all the test conditions, Fig. 1 (a) revealed a minimal weight change in the conditioned RIM R135 epoxy resin, which suggested almost no moisture absorption. This result was expected due to the relatively high viscosity of the resin and low hydrophilicity of the bisphenol-A chemistry, which prevented moisture absorption. On the contrary, a significant moisture absorption was displayed by the amine-based curing agent RIM H1366, as shown in Fig. 1 (b). This result was attributed to the low viscosity of the curing agent and the hydrophilic nature of the amine groups in the curing agent that allowed the absorption of the surface moisture deposition. A maximum moisture content of 12% relative to the initial weight was observed in the RIM H1366 when exposed to 38 °C at 90% RH. Relatively lower moisture content was recorded for other test conditions, as summarized in Table 1. The cure kinetics of the resin/curing agent mixture was then evaluated using DSC for the six case studies of 50% and 90% relative humidity, each at 5 °C, 23 °C, and 38 °C.

2.2. Cure kinetic law

The impact of moisture content on the resin cure kinetics was experimentally characterized using DSC (Discovery, TA Instruments). Dynamic scans were performed on the uncured mixture (100:30 parts by weight) sealed in a hermetic aluminum pan. Each DSC specimen weighed approximately 5 mg. The DSC specimens were first equilibrated at −10 °C within the DSC chamber for two minutes to avoid premature curing. The chamber temperature was then increased from the equilibration temperature to 250 °C at three different temperature rates of 5 °C/min, 10 °C/min, and 15 °C/min. The exothermic heat of the reaction of the curing resin was measured as a function of time and temperature for each dynamic scan, as seen in Fig. 2(a). The instantaneous heat of reaction, dH/dT, was obtained as the normalized heat flow at any given time, t. The partial heat of reaction, $H(t)$, up to time t, and the total heat of reaction, H_T, were computed by integrating the area under the normalized heat flow versus time plots up to time t and the end of the reaction, respectively.

The rate of curing, $d\phi/dt$, and the degree of cure, ϕ, for each temperature ramp were then calculated based on dH/dt at any time t and H_T given off by the curing thermoset as per Eqs. (1) and (2), respectively.

$$\frac{d\phi}{dt} = \frac{1}{H_T}\frac{dH}{dt} \tag{1}$$

$$\phi(t) = \frac{1}{H_T}\int_0^t \frac{dH}{dt}dt = \frac{H(t)}{H_T} \tag{2}$$

The rate and degree of cure obtained from Eqs. (1) and (2) were fitted to the autocatalytic Prout-Tompkins phenomenological kinetic model

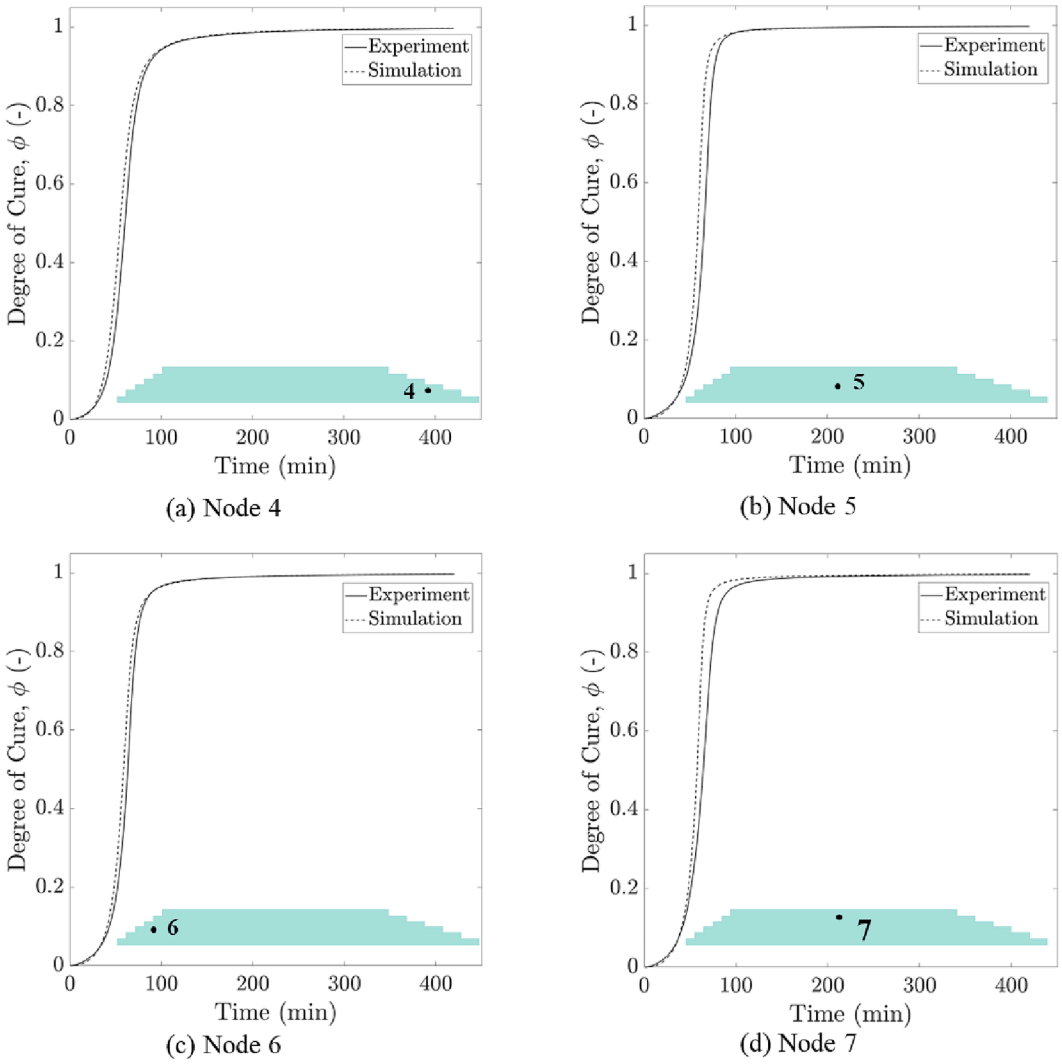

Fig. 7. Plots of the degree of cure evolution in the repair patch as a function of the time for (a) node 4, (b) node 5, (c) node 6, and (d) node 7 from experiments and numerical model. (For interpretation of the references to colour in this figure legend, the reader is referred to the web version of this article.)

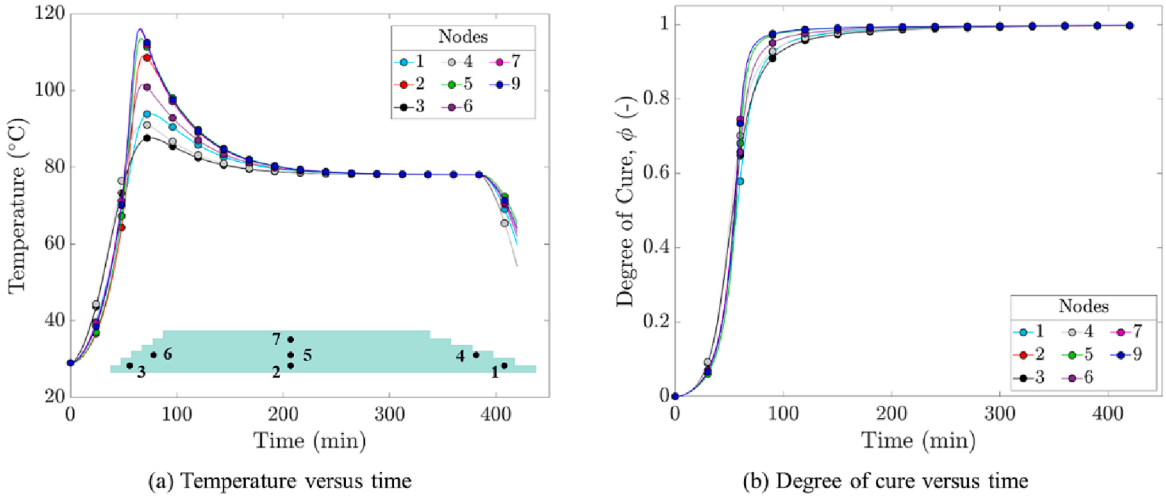

Fig. 8. (a) Temperature and (b) degree of cure profiles for all nodes in blade repair simulation. (For interpretation of the references to colour in this figure legend, the reader is referred to the web version of this article.)

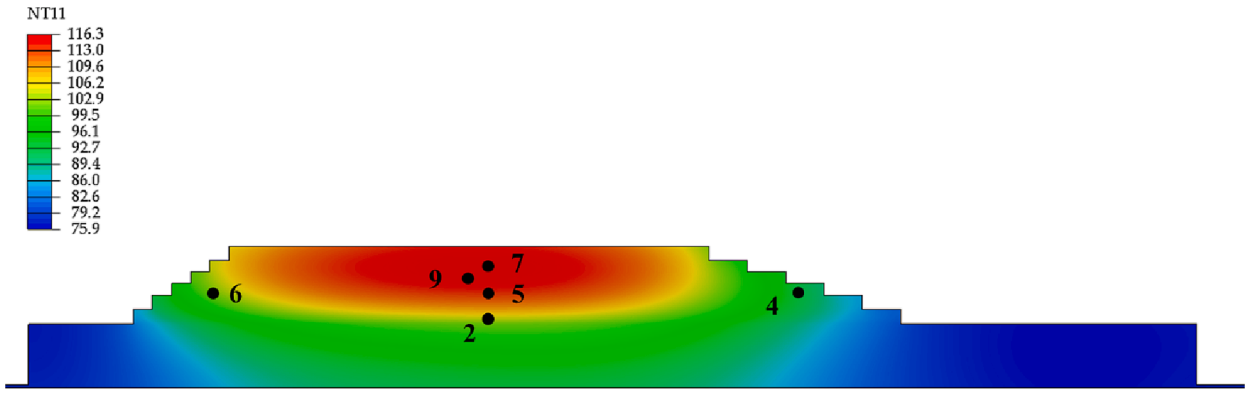

Fig. 9. Nodal temperature contour plot of repair patch showing the thermocouple nodes 2, 4, 5, 6, and 7, as well as node 9 experiencing the maximum exotherm at 66 min into curing. (For interpretation of the references to colour in this figure legend, the reader is referred to the web version of this article.)

Table 4
Numerical (experimental) peak exothermic temperature, time to peak exothermic temperature, the temperature at the end-of-cure, and time to degree of cure $\phi = 0.99$ for thermocouple nodes 1–7 and node 9 when no moisture was considered.

Nodes	Peak exotherm (°C)	Time to peak exotherm (min)	End-of-cure temperature (°C)	Time to $\phi = 0.99$ (mins)
1	87.7 (–)	75 (–)	54.2 (–)	225 (–)
2	109.1 (113.1)	69 (85)	65.4 (67.45)	168 (224)
3	94 (–)	75 (–)	59.8 (–)	249 (–)
4	91.2 (96.2)	69 (73.7)	54.4 (60.2)	237 (244)
5	113.7 (122.2)	66 (78.3)	65.4 (66.4)	153 (132)
6	101.5 (109.5)	69 (74.3)	61.9 (66)	198 (192)
7	116.1 (111.6)	66 (77.3)	63.2 (64.9)	147 (180)
9	116.3 (–)	66 (–)	64.1 (–)	144 (–)

[38,39] per ASTM E2890 [40] to determine the kinetic constants,

$$\frac{d\phi}{dt} = A\exp\left(-\frac{E_a}{RT^*}\right)[\phi^m(1-\phi)^n] \quad (3)$$

In Eq. (3), four material-specific parameters, namely the activation energy E_a, pre-exponential factor A, and the dimensionless modeling parameters m and n, were determined through a data-fitting procedure from the experimental data. Here, R is the universal gas constant and T^* is the absolute temperature in Kelvins. An in-house data-fitting tool was developed using MATLAB to perform nonlinear least-square analyses of the experimental data to determine the material-specific kinetic constants. The Kissinger method [38–40] was used to provide initial estimates for E_a and A [6,9] and the MATLAB "*lsqnonlin*" function was used for fitting. The best fits obtained for all temperature rates yielded the kinetic constants summarized in Table 2. The predictions of the degree of cure as a function of time, $\phi(t)$, for the unconditioned specimen calculated using the Prout-Tompkins model were compared to those from a previous study [9]. That study employed the Kamal-Sourour kinetic model, whose model predictions were compared with the experimentally measured degree of cure from the DSC re-runs of partially cured specimens. The Prout-Tompkins model predictions from the present study agreed very well with Kamal-Sourour kinetic model and the experimental data from the previous study [9], thus validating the Prout-Tompkins kinetic model.

The DSC tests and the data fitting procedure to determine the cure kinetics were repeated for conditioned specimens with varying moisture contents up to 12% (three specimens per moisture content). Deionized water was added to the resin mixture to condition the specimens in an amount corresponding to the values summarized in Table 1. Results for the maximum moisture content case of 12% are presented in Fig. 2(b) and compared with those of the unconditioned specimens. The unconditioned specimens manifested a relatively higher exothermic peak spread over a narrower temperature range than the 12% moisture content, as summarized in Table 2. Furthermore, adding 12% moisture reduced the activation energy, E_a, and the pre-exponential factor, A, (see Table 2). Lower activation energy and pre-exponential factors indicated that the reaction required less energy input to begin autocatalyzing and a shorter time to approach exponential growth, beyond which the cure reaction slowed down. Fig. 3 compares the degree of cure evolution of the unconditioned specimen as a function of time with the conditioned specimens with varying moisture contents for a prescribed cure cycle. Fig. 3 shows that the degree of cure evolution is accelerated with increased moisture content. While the unconditioned specimen required 250 mins to achieve a full cure state ($\phi = 1$) with the prescribed temperature profile, the resin with 12% moisture content cured in 100 mins for the same cycle. These trends were consistent with the findings of Sharp et al. [26]. They reported an increase in molecular diffusion in uncured epoxy due to moisture, which led to an accelerated cure. However, after sufficient crosslinks had formed, the moisture in the epoxy formed pockets that hindered further molecular diffusion, significantly reducing the cure rate. The cure kinetics, derived as a function of moisture content, can be used to understand the effect of moisture on the curing of wind blade repair patches, as described in Section 3.

2.3. Process modeling of blade repair

Process modeling, a physics-based numerical framework for simulating the curing process of composite materials, was employed for analyzing a composite laminate representative of a typical wind turbine blade repair [1]. Such models provide critical insight into the effect that the constituent materials, cure cycle, geometry, and boundary conditions have on the thermal and, by extension, cure histories during a blade repair procedure. Hence, with a well-calibrated model, optimization of the chosen repair curing protocols can be pursued to both reduce processing time and avoid exceeding temperature thresholds that will degrade the composite.

2.3.1. Manufacturing the representative repair patch

The representative laminate, manufactured in-house and consisting of E-glass fibers infused with RIM R135-H1366 epoxy resin, was designed with the goal of emulating geometrical features typical of blade repair patches. It featured a 200 mm base layer with asymmetrically stacked plies, resulting in a 23 mm thick composite laminate. The asymmetrical stacking sequence and layer-by-layer width dimensions

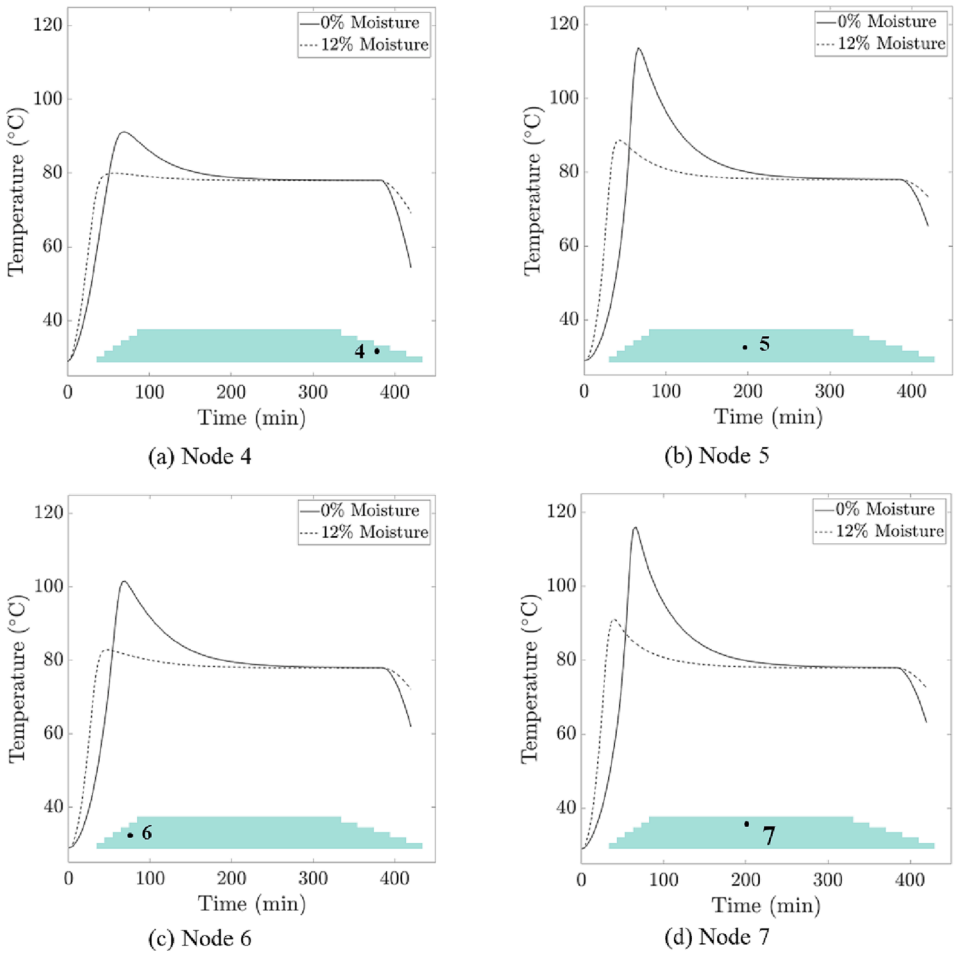

Fig. 10. Plots of temperature evolution in the repair patch as a function of the time and moisture content for (a) node 4, (b) node 5, (c) node 6, and (d) node 7. (For interpretation of the references to colour in this figure legend, the reader is referred to the web version of this article.)

precipitated two distinct scarfing slopes: 1:1 and 2:1. The two key features of the patch under consideration, the patch thickness and scarfing slope, were selected to better understand the effect of (a) scarf slope on thermal and cure histories with the material, and (b) patch thickness on curing reaction thermal gradients induced by the curing reaction exotherm. A schematic of the repair patch geometry and its dimensions are provided in Fig. 4. Note that the scarfing surfaces were not smoothened flat after manufacturing as shown in the schematic.

The composite repair patch was mounted on a borosilicate glass plate and cured in a convection oven. Several thermocouples were embedded along the centerline (through-thickness) of the laminate and along the scarfed regions to monitor the temperature evolution spatially within the composite during curing. An additional thermocouple was also placed in the oven, external to the patch, to track the oven temperature throughout the repair process to inform prescription of boundary conditions necessary for process modeling. Specific locations of each thermocouple location can be found in Fig. 4.

2.3.2. Numerical model

The process model was developed and interfaced with the commercial FE software Abaqus/STANDARD through user-written subroutine UMATHT. To capture the physics of the curing process virtually (i.e., the state-based evolution of cure and temperature), the model was governed by the Fourier heat law of thermal conduction shown in Eqs. (4) and (5) and the Prout-Tompkins kinetic model described above.

$$\rho^c c_P^c \frac{\mathrm{d}T}{\mathrm{d}t} = k^c \nabla^2 T + \dot{Q} \tag{4}$$

$$\dot{Q} = V^m \rho^m H_T^m \frac{\mathrm{d}\phi}{\mathrm{d}t} \tag{5}$$

Here, ρ^c, c_P^c and k^c are the composite density, specific heat capacity, and thermal conductivity of the curing patch, respectively; T is the temperature; $\dot{Q}$ is the rate of heat generated due to the reaction exotherm; $\mathrm{d}\phi/\mathrm{d}t$ is the rate of the resin curing reaction; and V^m, ρ^m and H_T^m are the resin volume fraction, density, and total enthalpy of the reaction, respectively. The composite properties were homogenized using the rule of mixtures [41].

Furthermore, the thermal properties of resin were assumed to vary linearly as a function of the degree of cure.

$$c_p = c_p^0 + \phi^*(c_p^1 - c_p^0) \tag{6}$$

$$k = k^0 + \phi^*(k^1 - k^0) \tag{7}$$

where c_p^0 and k^0 are the specific heat capacity and thermal conductivity of the uncured resin, respectively, and c_p^1 and k^1 are the specific heat capacity and thermal conductivity for the fully cured resin, respectively.

All components of the repair patch manufactured in the lab as shown in Fig. 4 (e.g., glass plate, vacuum bagging) were virtually reconstructed and meshed within Abaqus as presented in Fig. 5. The mesh consisted of 36753 DC3D8, eight-node linear heat transfer elements. Material properties for each component in the assembly and for the constituent composite materials are summarized in Table 3. Note that the manufactured laminate was measured to have a fiber volume fraction V^f =

Table 5
Peak exothermic temperature, time to peak exothermic temperature, the end-of-cure temperature, and time to degree of cure $\phi = 0.99$ for thermocouple nodes 1–7 and node 9 for all cases of moisture contents.

Moisture content	Nodes	Peak exotherm (°C)	Time to peak exotherm (min)	End-of-cure temperature (°C)	Time to $\phi = 0.99$ (mins)
0 %	1	87.7 (–)	75 (–)	54.2 (–)	225 ()
	2	109.1 (113.1)	69 (85)	65.4 (67.45)	168 (224)
	3	94 (–)	75 (–)	59.8 (–)	249 (–)
	4	91.2 (96.2)	69 (73.7)	54.4 (60.2)	237 (244)
	5	113.7 (122.2)	66 (78.3)	65.4 (66.4)	153 (132)
	6	101.5 (109.5)	69 (74.3)	61.9 (66)	198 (192)
	7	116.1 (111.6)	66 (77.3)	63.2 (64.9)	147 (180)
	9	116.3 (–)	66 (–)	64.1 (–)	144 (–)
2 %	1	88.9	81	71.3	174
	2	99.1	75	73.4	147
	3	84.7	78	69.3	183
	4	87.0	72	69.3	174
	5	101.7	72	73.4	141
	6	93.7	72	72.1	159
	7	103.0	69	72.6	138
	9	103.2	69.0	72.9	138
7 %	1	84.8	72	71.3	273
	2	92.7	63	73.4	240
	3	81.9	75	69.3	285
	4	83.5	66	69.3	276
	5	95.3	57	73.4	228
	6	88.5	60	72.1	258
	7	97.2	57	72.6	225
	9	97.2	57	72.9	225
9 %	1	81.1	69	71.3	87
	2	86.5	54	73.3	78
	3	79.5	75	69.2	87
	4	80.3	60	69.3	84
	5	88.4	48	73.3	75
	6	83.2	51	72.1	81
	7	90.5	45	72.5	72
	9	90.3	45	72.9	72
10 %	1	82.0	63	71.3	87
	2	89.0	45	73.4	75
	3	80.0	66	69.2	93
	4	81.2	51	69.3	87
	5	91.9	39	73.3	69
	6	85.2	45	72.1	81
	7	94.7	39	72.5	66
	9	94.5	39	72.9	66
12 %	1	80.8	66	71.3	75
	2	86.6	48	73.3	66
	3	79.2	72	69.2	75
	4	80.0	57	69.3	72
	5	88.8	42	73.3	63
	6	82.9	48	72.1	69
	7	91.2	39	72.5	60
	9	90.9	39	72.9	60

0.52.

Thermal boundary conditions were prescribed to the model to mimic the curing process inside a convection oven. Nominally, a temperature ramp from room temperature to 80 °C at 1.5 °C/min, followed by an isothermal hold at 80 °C for 350 mins, ending with passive cooling to ambient conditions after removal from the oven were prescribed for the curing analysis. The exact prescribed temperature profile was informed from the thermocouple placed in the convection oven separate from the repair patch as noted above. This thermal profile was prescribed directly to the modeled oven rack, and provided as convective boundary conditions to the faces of the model exposed to forced airflow inside the oven (from right to left relative to the patch model). The convective coefficients of air, denoted as h_1, h_2, and h_3 in Fig. 5, were estimated from typical values found in engineering literature [42,43] as 5 W/m^{2}K, 10 W/m^{2}K, and 15 W/m^{2}K, respectively.

3. Modeling results and experimental validation

The repair patch was manufactured in the laboratory to validate the process modeling predictions. Thermocouples were embedded in the laminate to record temperature data throughout the patch and assess the spatial variation in the temperature due to the exothermic heat of the reaction and the resulting degree of cure, as shown in Fig. 4. Temperature data during curing was compared to the numerical model predictions of the nodal temperature in four locations, as shown in Fig. 5. Fig. 6 compares the temperature evolution at specific nodes (4–7) from the virtual repair to the corresponding thermocouple data. Numerical model predictions agreed very well with the thermocouples read. Minor deviations in the magnitude and time to peak temperature were observed, which could be attributed to small imprecisions in defining the location of the thermocouple with respect to the computational nodes. The degree of cure evolution was computed from the temperature evolution data presented in Fig. 6 per the Prout-Tompkins kinetic model in Equation (3), as shown in Fig. 7.

3.1. Effect of scarf geometry on blade repair

Two distinct scarfing slopes of 1:1 and 2:1 were analyzed to evaluate the influence of the scarf geometry on the temperature and cure distribution. Fig. 8(a) presents an overlay of the temperature evolution at several nodes considered in this study. The plot clearly shows a spatial variation in the temperature within the repair patch. This spatial variation is also evident from the FE contour plot shown in Fig. 9. Peak temperature, time to peak temperature, and end-of-cure temperature are quantified as summarized in Table 4. In Table 4, node 5 reported a peak temperature of 113.7 °C while node 2 reported the lowest peak temperature of 109.1 °C. Such a temperature variation was attributed to the repair patch geometry, where the cure reaction was initiated at the center of the patch, close to node 5. Thus, the center experienced maximum peak exothermic temperatures. This heat was conducted outwards from the center resulting in lower peak temperatures at other nodes. Given the asymmetrical geometry of the patch, node 4 (2:1 slope) presented a distinct temperature profile with a peak temperature of 91.2 °C compared to node 6 (1:1 slope), where the peak temperature was 101.5 °C. Such variations were also attributed to the geometry of the patch, with node 4 being further away from the center and, consequently, reporting a lower temperature. Nodes 1 and 3 manifested a similar trend as nodes 4 and 6. To further illustrate the influence of the asymmetrical scarfing slope, the temperature of node 9 was also monitored. Note that node 9 was not along the centerline but was 2 mm to the left of the centerline. Node 9 reported the maximum peak temperature of any node within the repair patch, suggesting that the peak exothermic reaction did not initiate along the centerline of the repair but was 2 mm to its left. The uneven scarfing slopes shifted the peak exotherm from the centerline towards the steeper slope, suggesting that the repair geometry had a significant influence on the temperature evolution within the repair. Additionally, the time to peak temperature, as seen in Fig. 8(a) and Table 4, increased from 66 mins for node 5 to 75 mins for node 1 as the distance of the node increased from the centerline, indicative of a temperature lag in the repair patch.

This temperature lag was further evident from the end-of-cure temperature values. Nodes 2, 5, and 7 reported elevated end-of-cure temperatures (> 62 °C) compared to nodes 1, 3, 4, and 6 which were much closer to the prescribed cure cycle temperature.

The computed degrees of cure for the analyzed nodes are overlaid in Fig. 8(b). The degree of cure profiles followed the same trends as the temperature, as expected. Nodes closer to the centerline (nodes 2, 5, 7) were expected to cure faster than the nodes further away from the center (nodes 1, 3, 4, 6) because of their position with respect to the exothermic

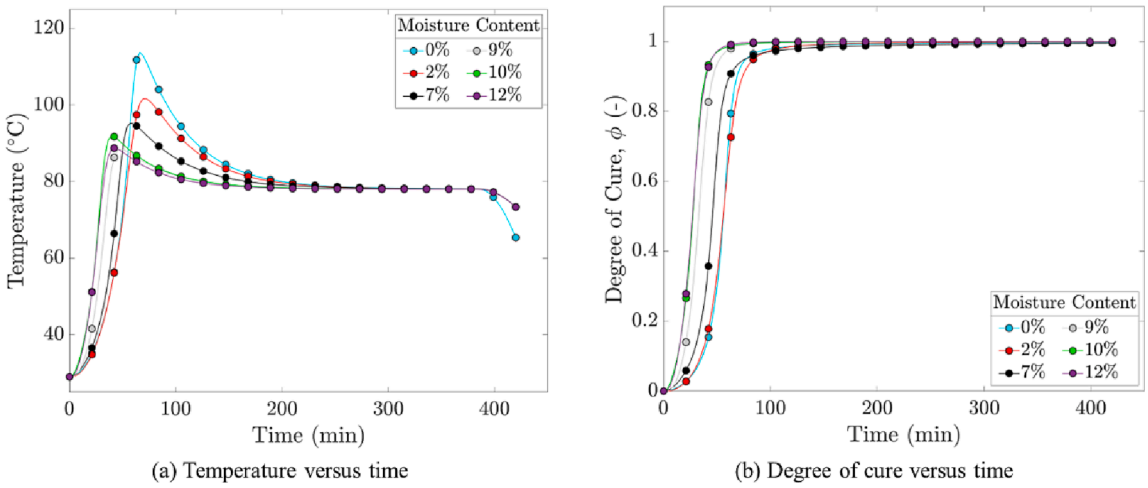

(a) Temperature versus time (b) Degree of cure versus time

Fig. 11. (a) Temperature and (b) degree of cure profiles for node 5 for six different moisture absorption cases. (For interpretation of the references to colour in this figure legend, the reader is referred to the web version of this article.)

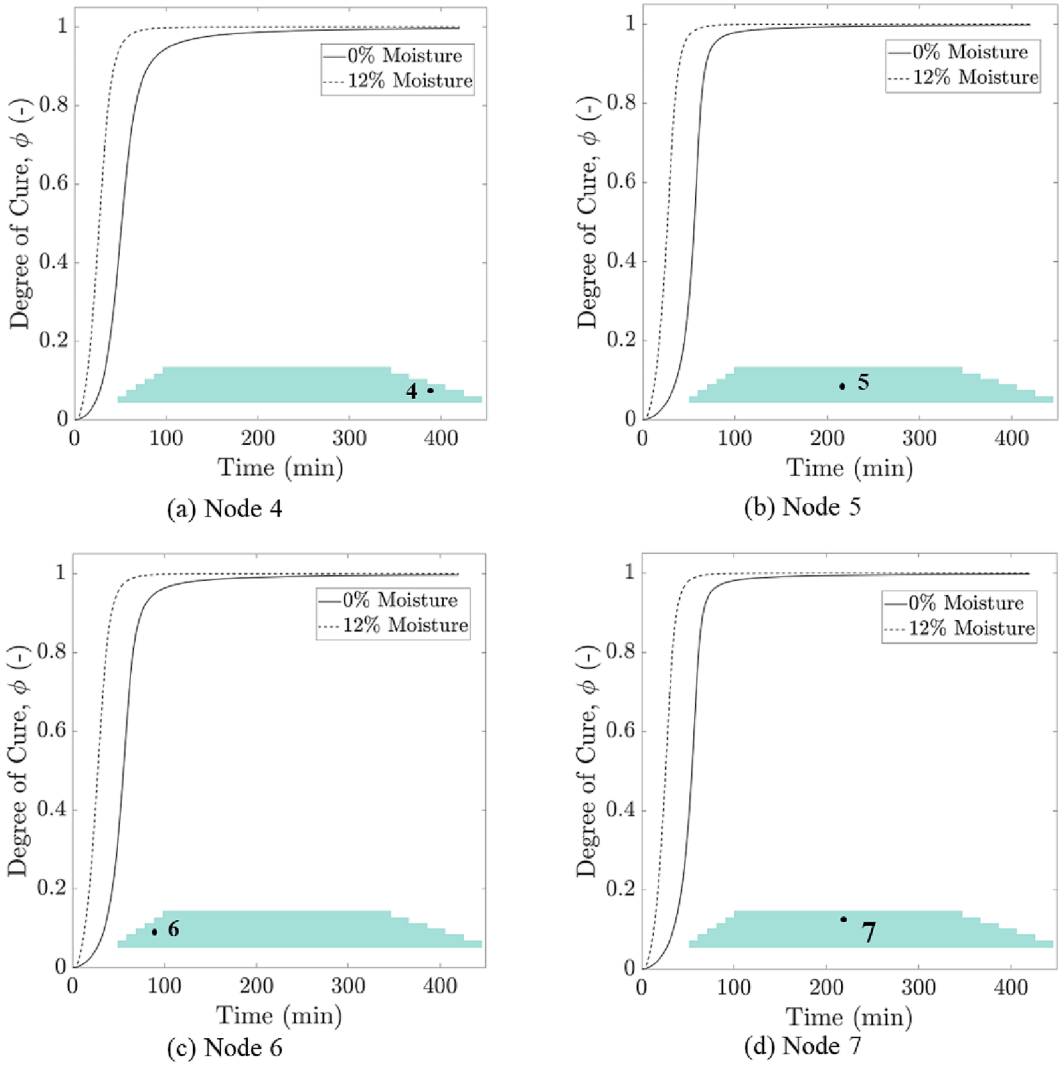

(a) Node 4 (b) Node 5

(c) Node 6 (d) Node 7

Fig. 12. Plots of the degree of cure evolution in the repair patch as a function of the time and moisture content for (a) node 4, (b) node 5, (c) node 6, and (d) node 7. (For interpretation of the references to colour in this figure legend, the reader is referred to the web version of this article.)

peak of the reaction. This observation was also evident from Table 4, which summarizes the time taken for each node to reach a complete cure of $\phi = 1$ (indicative of repair time). Node 5 achieved full cure in 153 mins compared to node 2 which reached full cure last after 168 mins. Node 9, which was expected to be closest to the peak exotherm, reached full cure in 144 mins. Nevertheless, all nodes within the laminates reached full cure well before the end of the recommended cure cycle.

3.2. Effect of moisture on blade repair

In the previous sections, the process modeling of a repair scarf laminate was validated against experimental results, and the influence of the repair geometry was evaluated. The effect of moisture content in the resin on temperature and degree of cure evolutions within the patch were evaluated using the same geometry and process modeling technique detailed in Section 2. Various moisture levels, summarized in Table 1, were considered. The corresponding kinetic modeling parameters from Table 2 were used to predict the temperature evolution and degree of cure in the repair patch for different moisture contents. An overlay plot of temperature evolution at several nodes of interest is presented in Fig. 10 as a function of the minimum and maximum moisture contents. The influence of moisture on the temperature evolution at nodes 4,5,6, and 7 can be observed in Fig. 10; results are also summarized in Table 5 in terms of peak temperature, time to peak temperature, and end-of-cure temperature. For instance, the temperature profile at node 5 for several moisture levels is presented in Fig. 11 (a). The exothermic peak shifted to shorter times from 66 mins for no moisture case to 42 mins for 12% moisture case, indicating an acceleration in the cure reaction with the moisture content. As previously mentioned, adding moisture increases molecular diffusion and dramatically reduces the reaction's activation energy, leading to an early onset of the cure reaction. Concurrently, the magnitude of the peak exothermic temperature dropped with increasing moisture content. Node 5 reported a peak temperature of 113.7 °C when no moisture was considered. However, this value dropped to 88.8 °C for the 12% moisture case. This drop in the peak temperature was attributed to the reduced total heat of the reaction with increasing moisture content reported in Table 2. This trend of accelerated cure and reduced peak temperatures with increasing moisture content was consistent for all the nodes considered in Fig. 10 (see Table 5). No significant influence of moisture was observed on the end-of-cure nodal temperature.

The computed degree of cure for all the nodes of interest as a function of moisture content is presented in Fig. 12 and the results are summarized in Table 5. The degree of cure plots exhibited similar and consistent trends to the temperature plots, where the cure rate significantly increased with the increased moisture content. Looking at node 5, for example, the degree of cure started approaching exponential growth after 39 mins of curing when no moisture was considered. By contrast, the 12% moisture case reported the beginning of an exponential cure rate after 12 mins. The faster cure reaction is attributed to enhanced molecular diffusion due to the added moisture [26]. However, after approaching a cure level of approximately 0.89, the cure reaction plateaued for all moisture levels due to the formation of moisture pockets within the free volumes of the crosslinked epoxy [26]. At that point, moisture pockets hindered further molecular diffusion and significantly reduced the reaction rate. However, the epoxy continued to cure until it reached a complete cure. Node 5 achieved full cure after 153 mins when no moisture was added. By contrast, the 12% moisture case took only 63 mins to cure fully. Similar values of time to fully cure were reported for other nodes of interest, as summarized in Table 5.

The results presented in this work show that epoxies can absorb a substantial amount of moisture during repairs, which can significantly alter their curing kinetics and affect the evolution of temperature and degree of cure within the repair patch. Furthermore, it was found that the scarfing angle also influenced the spatial variation of the temperature and cure evolution during the repair, with steeper slopes curing faster.

Numerical models, like the one presented in this study, can provide an in-depth understanding of the influence of such geometrical and environmental variables on the quality of the repair. Processing conditions, such as heating rates, hold temperatures, and multi-step cure cycles, can be varied, and their influence on the spatial variation of temperature and cure can be analyzed. Considering several parameters, an optimized cure cycle specific to a repair can be determined through the numerical approach presented in this study to ensure even curing in the shortest time.

4. Conclusions

This study investigated the influence of environmental moisture on the curing of wind blades during structural repairs. First, the moisture absorption in repair conditions was quantified by individually exposing the polymer and hardener to moisture. It was shown that the curing agent of the two-part resin system absorbed up to 12% moisture by weight when exposed to high temperature and relative humidity. Then, the effect of the moisture on cure kinetics was established by DSC tests. Tests showed that moisture intake significantly accelerated the cure reaction. The effect of altered cure kinetics and repair geometry on the repair time was investigated numerically through FE-based process modeling. The numerical model predictions were validated against a small-scale repair manufactured in the lab in terms of the temperature, degree of cure, and time to complete the repair. It was clear from this study that environmental factors, the size and type of repair involved, and the resin system utilized all play a crucial role in the cure and temperature evolution within the repair, thus making no two repairs alike.

Due to the large number of variables involved, there is a critical need for qualitative and quantitative predictive tools for evaluating optimized cure cycles for each repair. Numerical models, like the one presented in this study, can be used to optimize cure cycles to ensure a rapid, uniform degree of cure throughout the repair. This experimentally validated computational approach will be integrated within an ICME framework for curing-induced residual stress prediction, ultimately enabling a complete connection between materials, reaction kinetics, and mechanical performance.

CRediT authorship contribution statement

Sagar P. Shah: Conceptualization, Methodology, Validation, Investigation, Writing – original draft, Writing – review & editing, Visualization. **Michael N. Olaya:** Methodology, Software, Validation, Formal analysis, Investigation, Writing – review & editing. **Evgenia Plaka:** Methodology, Validation, Formal analysis, Investigation, Writing – original draft. **Joseph McDonald:** Methodology, Validation, Formal analysis, Writing – original draft. **Christopher J. Hansen:** Methodology, Validation, Writing – review & editing, Supervision. **Marianna Maiarù:** Conceptualization, Methodology, Validation, Writing – review & editing, Resources, Supervision, Project administration, Funding acquisition.

Declaration of Competing Interest

The authors declare that they have no known competing financial interests or personal relationships that could have appeared to influence the work reported in this paper.

Data availability

No data was used for the research described in the article.

Acknowledgments

This paper is based upon work partially supported by the National Science Foundation under grant numbers 1362022, 1362023, 1916715, and 1916776 (i/UCRC for Wind Energy, Science, Technology, and Research) and from the members of WindSTAR I/UCRC. Any opinions, findings, and conclusions or recommendations expressed in this material are those of the author(s) and do not necessarily reflect the view of the Nation Science Foundations or the sponsors. The authors would also like to thank the WindSTAR Industrial Advisory Board members Steve Nolet and Amir Salimi (TPI Composites); Nathan Bruno, Mirna Robles, and Paul Ubrich (Westlake Epoxy); Ben Rice (Pattern Energy); and Jian Lahir (EDPR) for their technical advice and support and for providing the resin for experimental investigation.

References

[1] Katnam KB, Comer AJ, Roy D, da Silva LFM, Young TM. Composite Repair in Wind Turbine Blades: An Overview. J Adhes Jan. 2015;91(1–2):113–39. https://doi.org/10.1080/00218464.2014.900449.
[2] Mishnaevsky L, Branner K, Petersen H, Beauson J, McGugan M, Sørensen B. Materials for Wind Turbine Blades: An Overview. Materials Nov. 2017;10(11):1285. https://doi.org/10.3390/ma10111285.
[3] Mishnaevsky L, Frost-Jensen Johansen N, Fraisse A, Fæster S, Jensen T, Bendixen B. Technologies of Wind Turbine Blade Repair: Practical Comparison. Energies Jan. 2022;15(5). https://doi.org/10.3390/en15051767. Art. no. 5.
[4] Li M. Temperature and moisture effects on composite materials for wind turbine blades. Bozeman Montana: Montana State University-Bozeman; 2000.
[5] Candela Garolera A, Madsen SF, Nissim M, Myers JD, Holboell J. Lightning Damage to Wind Turbine Blades From Wind Farms in the U.S. IEEE Trans Power Deliv Jun. 2016;31(3):1043–9. https://doi.org/10.1109/TPWRD.2014.2370682.
[6] Olaya MN, Mcdonald J, Shah S, Hansen CJ, Stapleton SE, Maiaru M. Wind Blade Repair Optimization. In: Proceedings of the American Society for Composites — Thirty-fifth Technical Conference, Sep. 2020. Doi: 10.12783/asc35/34979.
[7] Mischnaewski L, Mishnaevsky L. Structural repair of wind turbine blades: Computational model for the evaluation of the effect of adhesive properties. Wind Energy Apr. 2021;24(4):402–8. https://doi.org/10.1002/we.2575.
[8] Mishnaevsky L. Repair of wind turbine blades: Review of methods and related computational mechanics problems. Renew Energy Sep. 2019;140:828–39. https://doi.org/10.1016/j.renene.2019.03.113.
[9] Shah SP, Patil SU, Hansen CJ, Odegard GM, Maiarù M. Process modeling and characterization of thermoset composites for residual stress prediction. MAMS 2021: 1–12, doi: 10.1080/15376494.2021.2017527.
[10] Anandan S, Dhaliwal GS, Huo Z, Chandrashekhara K, Apetre N, Iyyer N. Curing of Thick Thermoset Composite Laminates: Multiphysics Modeling and Experiments. Appl Compos Mater Oct. 2018;25(5):1155–68. https://doi.org/10.1007/s10443-017-9658-9.
[11] Bujun K. Processing Study of in-situ Bonded Scarf Repairs for Composite Structures. Montreal, Quebec: McGIll University; 2004.
[12] Cassano AG, Dev S, Maiaru M, Hansen CJ, Stapleton SE. Cure simulations of thick adhesive bondlines for wind energy applications. J Appl Polym Sci 2021;138(10):49989. https://doi.org/10.1002/app.49989.
[13] Heinrich C. The Influence of the Curing Process on the Response of Textile Composites. University of Michigan, Ann Arbor; 2011. [Online]. Available: https://hdl.handle.net/2027.42/84441.
[14] Li X, Wang J, Li S, Ding A. Cure-induced temperature gradient in laminated composite plate: Numerical simulation and experimental measurement. Compos Struct Dec. 2020;253:112822. https://doi.org/10.1016/j.compstruct.2020.112822.
[15] Loos A, Springer G. Calculation of Cure Process Variables During Cure of Graphite/Epoxy Composites. In: Composite Materials: Quality Assurance and Processing, C. Browning, Ed., 100 Barr Harbor Drive, PO Box C700, West Conshohocken, PA 19428-2959: ASTM International; 1983, pp. 110-110–9. doi: 10.1520/STP28542S.
[16] Nakouzi S, Pancrace J, Schmidt FM, Le Maoult Y, Berthet F. Curing Simulation of Composites Coupled with Infrared Heating. Int J Mater Form Apr. 2010;3(S1):587–90. https://doi.org/10.1007/s12289-010-0838-5.
[17] Darwish FH, Shivakumar KN. Experimental and Analytical Modeling of Scarf Repaired Composite Panels. Mech Adv Mater Struct Mar. 2014;21(3):207–12. https://doi.org/10.1080/15376494.2013.834096.
[18] Wang CH, Venugopal V, Peng L. Stepped Flush Repairs for Primary Composite Structures. J Adhes Jan. 2015;91(1–2):95–112. https://doi.org/10.1080/00218464.2014.896212.
[19] Wang CH, Gunnion AJ. On the design methodology of scarf repairs to composite laminates. Compos Sci Technol Jan. 2008;68(1):35–46. https://doi.org/10.1016/j.compscitech.2007.05.045.
[20] Soutis C, Hu FZ. Failure Analysis of Scarf-Patch-Repaired Carbon Fiber/Epoxy Laminates Under Compression. AIAA J Apr. 2000;38(4):737–40. https://doi.org/10.2514/2.1027.
[21] Shah SP, Maiarù M. Effect of Manufacturing on the Transverse Response of Polymer Matrix Composites. Polymers Jan. 2021;13(15):1–4. https://doi.org/10.3390/polym13152491. Art. no. 15.
[22] Maiaru M. Effect of uncertainty in matrix fracture properties on the transverse strength of fiber reinforced polymer matrix composites. In: 2018 AIAA/ASCE/AHS/ASC Structures, Structural Dynamics, and Materials Conference, American Institute of Aeronautics and Astronautics; 2018. doi: 10.2514/6.2018-1901.
[23] Maiarù M, D'Mello RJ, Waas AM. Characterization of intralaminar strengths of virtually cured polymer matrix composites. Compos B Eng Sep. 2018;149:285–95. https://doi.org/10.1016/j.compositesb.2018.02.018.
[24] Aktas L, Hamidi Y, Altan MC. Effect of Moisture Absorption on Mechanical Properties of Resin Transfer Molded Composites. In: Materials: Processing, Characterization and Modeling of Novel Nano-Engineered and Surface Engineered Materials, New Orleans, Louisiana, USA: ASMEDC, Jan. 2002, pp. 173–181. 10.1115/IMECE2002-39223.
[25] Choi S, Janisse AP, Liu C, Douglas EP. Effect of water addition on the cure kinetics of an epoxy-amine thermoset. J Polym Sci A Polym Chem 2011;49(21):4650–9. https://doi.org/10.1002/pola.24909.
[26] Sharp N, Li C, Strachan A, Adams D, Pipes RB. Effects of water on epoxy cure kinetics and glass transition temperature utilizing molecular dynamics simulations. J Polym Sci B 2017;55(15):1150–9. https://doi.org/10.1002/polb.24357.
[27] Shen C-H, Springer GS. Moisture Absorption and Desorption of Composite Materials. J Compos Mater 1976;10.
[28] Kropka JM, Adolf DB, Spangler S, Austin K, Chambers RS. Mechanisms of degradation in adhesive joint strength: Glassy polymer thermoset bond in a humid environment. Int J Adhes Adhes Dec. 2015;63:14–25. https://doi.org/10.1016/j.ijadhadh.2015.07.014.
[29] Patil S et al. Multi-scale Approach to Predict Cure-Induced Residual Stresses in an Epoxy System. In: Proceedings of the American Society of Composites 35th Technical (Virtual) Conference, American Society of Composites, Sep. 2020.
[30] Deshpande PP et al. Multiscale Modelling of the Cure Process in Thermoset Polymers Using ICME. In: Proceedings of the American Society for Composites " Thirty-fifth Technical Conference; 2020. Doi: 10.12783/asc35/34889.
[31] Odegard GM, et al. Molecular Dynamics Modeling of Epoxy Resins Using the Reactive Interface Force Field. Macromolecules Nov. 2021;54(21):9815–24. https://doi.org/10.1021/acs.macromol.1c01813.
[32] Shah S et al. Multiscale Modeling for Virtual Manufacturing of Thermoset Composites. In: AIAA Scitech 2020 Forum. In: AIAA SciTech Forum. American Institute of Aeronautics and Astronautics, Jan. 2020. Doi: 10.2514/6.2020-0882.
[33] Patil SU, Shah SP, Olaya M, Deshpande PP, Maiaru M, Odegard GM. Reactive Molecular Dynamics Simulation of Epoxy for the Full Cross-Linking Process. ACS Appl Polym Mater Oct. 2021. https://doi.org/10.1021/acsapm.1c01024.
[34] Gaikwad PS, et al. Understanding the Origin of the Low Cure Shrinkage of Polybenzoxazine Resin by Computational Simulation. ACS Appl Polym Mater Dec. 2021;3(12):6407–15. https://doi.org/10.1021/acsapm.1c01164.
[35] D'Mello RJ, Maiarù M, Waas AM. Effect of the curing process on the transverse tensile strength of fiber-reinforced polymer matrix lamina using micromechanics computations. Integrating Materials Dec. 2015;4(1):119–36. https://doi.org/10.1186/s40192-015-0035-y.
[36] Shah S, Maiaru M. Microscale Analysis of Virtually Cured Polymer Matrix Composites Accounting for Uncertainty in Matrix Properties During Manufacturing. In: American Society for Composites 2018, DEStech Publications, Inc., Nov. 2018. Doi: 10.12783/asc33/25958.
[37] D'Mello RJ, Waas AM, Maiaru M, Koon R. Integrated Computational Modeling for Efficient Material and Process Design for Composite Aerospace Structures. In: AIAA Scitech 2020 Forum, American Institute of Aeronautics and Astronautics, Jan. 2020. doi: 10.2514/6.2020-0655.
[38] Hardis R, Jessop JLP, Peters FE, Kessler MR. Cure kinetics characterization and monitoring of an epoxy resin using DSC, Raman spectroscopy, and DEA. Compos A Appl Sci Manuf Jun. 2013;49:100–8. https://doi.org/10.1016/j.compositesa.2013.01.021.
[39] Kissinger HE. Reaction Kinetics in Differential Thermal Analysis. Anal Chem Nov. 1957;29(11):1702–6. https://doi.org/10.1021/ac60131a045.
[40] "E2890-12(2018) Standard Test Method for Kinetic Parameters for Thermally Unstable Materials by Differential Scanning Calorimetry Using the Kissinger Method." ASTM International; 2018. [Online]. Available: https://doi.org/10.1520/E2890-12R18.
[41] Olaya MN, Maiaru M. A multi-scale approach for process modeling of polymer matrix composites. In: AIAA SCITECH 2022 Forum, American Institute of Aeronautics and Astronautics. doi: 10.2514/6.2022-0379.
[42] Kosky P, Balmer R, Keat W, Wise G. Chapter 12 - Mechanical Engineering. In: Kosky P, Balmer R, Keat W, Wise G, editors. Exploring Engineering (Third Edition). Boston: Academic Press; 2013, pp. 259–281. Doi: 10.1016/B978-0-12-415891-7.00012-1.
[43] Yener T, Yener ŞÇ, Mutlu R. Convection Coefficient Estimation of Still Air Using an Infrared Thermometer and Curve-Fitting. jetas, Aug. 2019; 4(2): Art. no. 2, doi: 10.30931/jetas.598862.